J. Hydrol. Hydromech., 72, 2024, 1, 34–48
https://doi.org/10.2478/johh-2023-0041
© 2024 Elnaz Bodaghi et al., published by Sciendo. This work is licensed under the Creative Commons Attribution-NonCommercial-NoDerivatives 4.0 International Licence.

sciendo Journal of Hydrology and Hydromechanics Institute of Hydrology SAS

Experimental investigation of scour downstream of a type A trapezoidal piano key weir under free and submerged flow conditions

Elnaz Bodaghi[1], Chonoor Abdi-Chooplou[2], Masoud Ghodsian[3*]

[1] Faculty of Civil and Environmental Engineering, Tarbiat Modares University, Tehran, Iran. E-mail: e.bodaghi@modares.ac.ir
[2] Faculty of Civil and Environmental Engineering, Tarbiat Modares University, Tehran, Iran. E-mail: a.chonoor@modares.ac.ir
[3] Faculty of Civil and Environmental Engineering, Tarbiat Modares University, Tehran, Iran. E-mail: ghods@modares.ac.ir
[*] Corresponding author. Tel.: 009882883317. E-mail: ghods@modares.ac.ir

Abstract: In this paper, the scour downstream of a trapezoidal Piano key weir (PKW) is investigated under free and submerged flow conditions. For this purpose, an experimental model was used in a laboratory channel with a length of 10 m, width of 0.75 m, and height of 0.8 m at various discharges and tailwater depths. The results showed an increase and decrease in the maximum scour depth with an increase in the discharge and submergence ratio, respectively. In addition, increasing the particle Froude number enhanced the geometric features of the scour hole downstream of the PKW. The rate of bed changes slowed down over time. The average values of maximum scour depth, the distance of the maximum scour depth from the weir toe, maximum scour hole length and weir toe scour depth increased in the free flow compared to the submerged flow. The scour hole volume and scour hole area in the submerged flow were less compared to the free flow. The average maximum level of the sedimentary ridge in the free flow is less than the submerged flow. New equations for calculating the geometric characteristics of the scour hole downstream of the trapezoidal PKW are presented with acceptable accuracy.

Keywords: Free flow; Particle Froude number; Piano key weir; Scouring; Submerged flow.

1 INTRODUCTION

Piano key weirs (PKWs) are a type of non-linear weirs that have been used due to their advantages, such as providing at least four times increase in specific discharge (up to 100 m^2/s) and lower maintenance costs, compared to linear weirs (Machiels, 2012). Generally, PKWs are of the following four types based on their upstream and downstream overhangs (Lempérière et al., 2011):

- Type A with upstream and downstream overhangs.
- Type B with only an upstream overhang.
- Type C with only a downstream overhang.
- Type D with no overhangs.

The first PKW was designed in 2001 and then built by Électrique de France in 2006 (Machiels et al., 2011). In the implementation phase, the French Ministry of Electricity modified the weir of the Goulours dam in 2006 and built the PKW (Laugier, 2007). After that, PKWs were employed to enhance the flood discharge capacities of the Marc, Etroit, and Gloriettes dams (Erpicum et al., 2011). Lempérière and Ouamane (2003) performed tests on the hydraulics of PKWs, followed by Hien et al. (2006), Barcouda et al. (2006), Ouamane and Lempérière (2006), Machiels et al. (2012), Kabiri-Samani and Javaheri (2012), Safarzadeh and Noroozi (2015), Karimi et al. (2019), and Abhash and Pandey (2021). Most of the studies focused on the hydraulics of PKWs, and limited research was performed on scouring downstream of these types of weirs, some of which are mentioned here. By conducting experiments on the scour downstream of a rectangular PKW under free flow conditions, Jüstrich et al. (2016) concluded that maximum scour depth depended on sediment characteristics, discharge, difference in the upstream and downstream flow heads, and tailwater depth. Dehrashid and Gohari (2019) investigated the effects of flow conditions and particle Froude number on the amount of scouring downstream of a rectangular PKW with an apron under free flow conditions. They demonstrated that the values of maximum scour depth, maximum scour hole length, and maximum scour depth location augmented with the increase of particle Froude number. By studying the scour downstream of trapezoidal and rectangular PKWs under free flow conditions, Yazdi et al. (2020) stated that the geometric characteristics of the scour hole were enhanced with an increase in discharge and a decrease in tailwater depth, and the scour depth was more in the rectangular compared to the trapezoidal weir. Kumar and Ahmad (2020) experimentally studied the effects of the apron on the scour downstream of a rectangular PKW under free-flow conditions. They showed that the apron decreases the scour depth. By investigating the scour downstream of a PKW with a zigzag lateral crest under free flow conditions, Moradi et al. (2020) showed a decrease in maximum scour depth. Ghodsian et al. (2021) revealed that average values of maximum scour depths downstream of a triangular PKW were higher than those of a trapezoidal PKW. Bodaghi et al. (2021) experimentally showed that by increasing tailwater depth and discharge, the scour depth downstream of a trapezoidal PKW decreases and increases under free flow conditions, respectively.

Kumar et al. (2021) investigated the movement of sediment particles on the inlet keys of a rectangular PKW under free-flow conditions. They observed that the speed of the sediment particles decreased by approaching the inlet key. However, the flow contraction and the rapid increase in shear stress caused a sudden acceleration in their movements through the inlet keys. Lantz et al. (2021) conducted an experimental study on the impacts of the weir apron and cut-off wall on the scour downstream of a rectangular PKW under free-flow conditions. They showed that a horizontal apron reduced the scour dimensions significantly.

Lantz et al. (2022) also analysed the temporal evolution of the scour downstream of a rectangular PKW under free-flow conditions. They observed three main phases of scour evolution. Abdi-Chooplou et al. (2022a) performed an experimental investigation on the temporal evolution of scouring downstream of a trapezoidal PKW. They showed that the scour rate enlargement occurred within the first 20% of the test durations. Abdi-Chooplou et al. (2022b) observed that the scour depth downstream of a trapezoidal PKW, under free flow, varies with the weir geometry. Abdi-Chooplou et al. (2023) numerically and experimentally investigated the influence of crest indentation on the flow field and scour downstream of rectangular PKWs. The preliminary experiments of Bodaghi et al. (2023), with a limited range of parameters, showed the reduction of scour downstream of a trapezoidal PKW in the submerged flow condition.

By reviewing the studies conducted on scouring downstream of PKWs, it is clear that almost all the earlier studies have been done under free-flow conditions. Although the weirs are usually designed for free flow, their submergence is possible, especially during floods. Submergence occurs when the tailwater level is higher than the weir crest level. This situation is possible for the weir as a diversion dam in a river. Considering the advantages of PKWs and insufficient studies on scouring under submerged flow conditions, it was necessary to conduct the relevant experiments. Therefore, in continuation of work of Bodaghi et al. (2023), in this experimental research, the temporal variations of scour parameters (including scour depth, changes in maximum scour depth and its location, longitudinal bed profiles, scour hole length, scour hole volume, scour hole area, and sedimentary ridge) downstream of a type-A trapezoidal PKW, at varied discharges and tailwater depths are investigated, under free and submerged flow conditions.

2 MATERIALS AND METHODS

2.1 Dimensional analysis

The geometric characteristics of scouring under free and submerged flow conditions, including maximum scour hole depth (d_{sm}), distance of location of maximum scour depth from the weir (L_{xm}), scour hole length (X_o), scour depth at the weir toe (Z_f), and maximum height of the sediment ridge downstream of the scour hole (h_{sm}) are presented in Fig. 1a and b. The geometric characteristics of a trapezoidal PKW as shown in Figs. 1c and 1d are weir height (P), total width (W), inlet key width (W_i), outlet key width (W_o), length of lateral walls (B), overhang length of the inlet keys (B_i), overhang length of the outlet keys (B_o), length of weir crest (L_w), and walls thickness (T_s). The parameters affecting the scour downstream of PKWs, including geometrical and hydraulic parameters, are as follows:

$$\psi = f_1\left(H,\ H_d,\ H_d^*,\ \rho,\ \rho_s, q, g, d_{50}, W,\ B,\ L_w,\ \sigma,\ \mu\right) \qquad (1)$$

In which f_1 is the functional symbol, ψ is the geometric characteristics of scour hole (i.e., d_{sm}, L_{xm}, X_o and Z_f), H is the upstream flow head over the weir, H_d is the downstream flow head, H^*_d is the downstream flow head relative to the weir crest under submerged condition, ρ is the specific mass of fluid, ρ_s is the specific mass of sediment particles, q is the unit discharge, g is the acceleration of gravity, d_{50} is the median size of sediment particles, σ is the surface tension of water, and μ is the dynamic viscosity of water. The approach depth of flow in all the experiments was greater than 0.03 m, so the surface tension effect was considered insignificant (Pfister et al., 2013). In addition, due to the presence of turbulent flow, the effect of viscosity is negligible (Ettema et al., 2000). By using the Buckingham

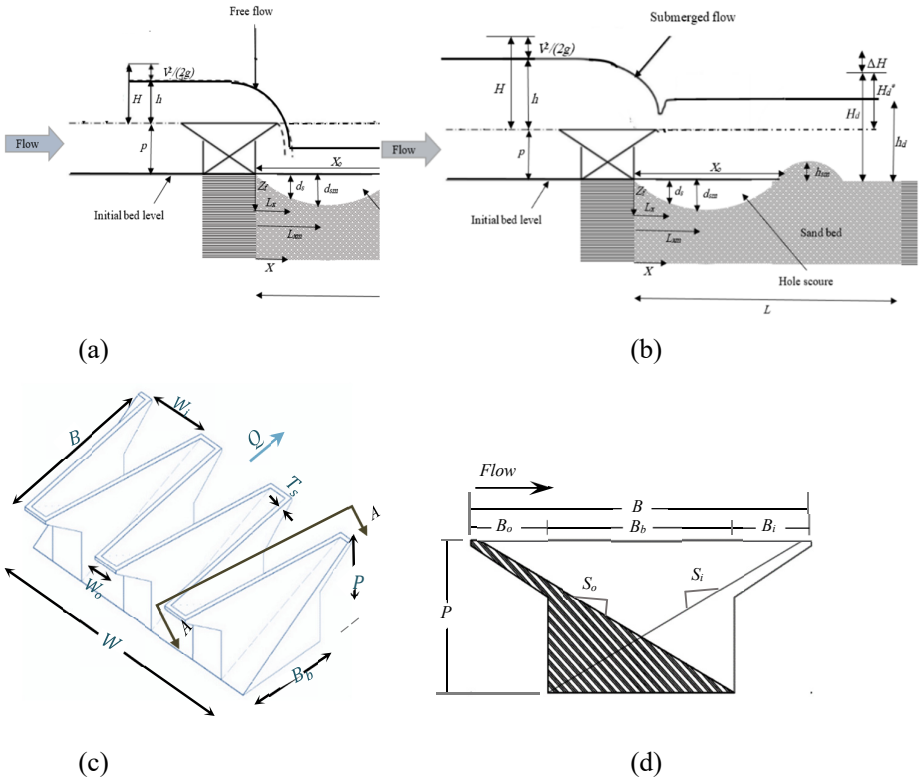


Fig. 1. Scour characteristics and hydraulic parameters under: a) Free flow, and b) Submerged flow, c) 3D view of PKW, and d) Section A-A.

Π theorem and considering H_d, q, and ρ as repeating variables, after eliminating the constant dimensionless variables (L_w/B, L_w/W and B/W), Eq. (2) was obtained:

$$\frac{\psi}{H}=f_2\left(\frac{d_{50}}{H_d},\frac{q}{\sqrt{gH_d^3}},\frac{\rho_s-\rho}{\rho},\frac{H_d}{H},\frac{H_d^*}{H}\right) \quad (2)$$

By combining independent variables $\frac{q}{\sqrt{gH_d^3}}$, $\frac{d_{50}}{H_d}$, and $Sc = \frac{\rho_s-\rho}{\rho}$ the particle Froude number $\mathrm{Frd} = (\frac{q}{H_d\sqrt{gd_{50}(Sc-1)}})$ was obtained. Therefore, Eq. (2) reduces as:

$$\frac{\psi}{H}=f_3(\mathrm{Frd},\frac{H_d}{H},S) \quad (3)$$

where f_2 and f_3 are functional symbols, and $S = H^*_d/H$ is the submergence ratio. Kabiri-Samani and Javaheri (2012) state that weir submergence will occur if $S \geq 0.6$. Dabling and Tullis (2012) presented this value as 0.48. For the free flow condition, the above equation further reduces as:

$$\frac{\psi}{H}=f_4\left(\mathrm{Frd},\frac{H_d}{H}\right) \quad (4)$$

in which f_4 is a functional symbol.

2.2 Experiments

The experiments were conducted in a rectangular channel with a length of 10 m, width of 0.75 m, and height of 0.8 m, with glass walls and horizontal bottom in the hydraulic laboratory of Tarbiat Modares University, Tehran. The trapezoidal PKW model was installed at a distance of about 3 m from the channel entrance. A type-A trapezoidal PKW model made of a thermo-plastic sheet with a thickness of 0.012 m was used. The weir had six keys with the same slopes as the inlet and output keys. The specifications of the used PKW are similar to those used by Abdi-Chooplou et al. (2022a).

The granulometry of the sedimentary bed is characterized by d_{10} = 1.35 mm; d_{50} = 2.2 mm; and d_{90} = 2.72 mm; leading to standard deviation of $\sigma_g = (d_{90}/d_{10})^{0.5} = 1.43 < 1.5$, which represent uniform sediment (Chiew, 1984; Chiew and Melville, 1989). The scale effect of scouring is negligible since $d_{10} > 1$ mm (Pagliara et al., 2006). The length of the erodible bed downstream of the weir was about 3 m, and the width and depth of the sediment layer were 0.75 and 0.425 m, respectively. The water is supplied from a pump to the channel entrance box. An ultrasonic flow meter (model TFM3100-F1) was used to measure the discharge with an accuracy of ±0.1 L/s. After installing the weir and sealing it, the sediments poured on the channel bottom, and its surface levelled with a bed flattener. A gate at the end of the channel adjusted the tailwater depth. The experiments were conducted for the free and submerged flow conditions. The upstream and downstream flow depths were measured using a digital point gauge with ±1 mm accuracy. Before the start of each text, a thin metal sheet was placed on the bed material, and then the discharge was adjusted using the ultrasonic flow meter. After stabilizing the flow, the test started by removing the metal sheet. After completing the test, the pump was switched off, and after draining the water, the bed topography was measured with a laser bed profiler with an accuracy of ±1 mm. The distances between the measuring points of the bed topography were 3 and 5 cm in the scour hole area and its downstream side, respectively.

The temporal variations of the longitudinal bed profile were recorded by a camera and digitized using digitizer software. The experiments were conducted for t_e = 300 min, in which the enlargement of the scour hole dimensions was insignificant, and an equilibrium state was achieved (Abdi-Chooplou et al., 2022a). The experiments were carried out for five discharges (i.e., 0.03, 0,.04, 0.05, 0.06, and 0.07 m^3/s), four tailwater for submerged flow (i.e., 0.23, 0.25, 0.27, and 0.29 m) and three tailwater depths for free flow (i.e. 0.08, 0.13, and 0.18 m). A total of 35 tests were carried out, the characteristics of which are presented in Table 1.

3 RESULTS AND DISCUSSION

This research investigates the characteristics of the scour hole downstream of a type-A trapezoidal PKW by changing the discharge and tailwater depth. Tailwater depths are adjusted in such a manner to have free and submerged flow conditions. Figure 2 shows the schematic of the flow pattern downstream of the submerged weir. The experiments revealed that a wavy water surface was formed downstream of the weir after impacting the outflow from the inlet keys to the tailwater surface under submerged flow conditions. The outflow from the inlet keys moved downward, forming a weak rotating zone downstream of the weir (Fig. 2a). The outflow from the outlet keys forms a submerged inclined jet followed by a strong rotational flow (Fig. 2b). Therefore, more scouring occurred downstream of the outlet keys.

The strength of the above-mentioned wavy water surface and the bed topography depends on the submergence ratio and approach flow conditions. Figure 3 displays the flow and bed topography downstream of the weir for two submergence ratios (i.e., S = 0.92 and 0.97) with $Q = 50\times10^{-3}$ m^3/s. A lower submergence ratio is associated with higher flow turbulence and surface undulations (Fig. 3–a). Increasing the submergence ratio decreased the strength of surface undulations and flow turbulence (Fig. 3–c). With increasing the submergence ratio, the flow hits the water surface with a lower velocity due to decreased drop height, leading to decreased bed changes. The reduction of the scour depth due to increased submergence is caused by increased diffusion length downstream of PKW, all other parameters being constant (Lantz et al., 2022). More specifically, the water depth plays a fundamental role in decreasing the shear stresses acting on the bed. Consequently, the active shear stress equals the critical counterpart for smaller scour depths in the case of higher tailwaters. Thus, in Fig. 3d, a scour hole with a smaller depth is clear compared to Fig. 3b.

Figure 4 shows temporal variations of the scour depth for different hydraulic conditions. The scouring begins when the weir outflow hits the downstream bed, and the scour hole dimension augment with time. It is clear that, in all the experiments, the rate of changes in scour depth was higher during the early stages of experimental duration, after which it decreased significantly until no changes were observed over time (Fig. 4). As the scour depth enhances, the scoring potential of the jet declines. Thus, the scour rate is more at the beginning and then decreases. When the jet's kinetic energy can no longer move the sediment particles, the scour hole reaches equilibrium (i.e., at t_e = 300 min).

Table 1. Test program.

Test No.	$Q\times10^{-3}$ (m^3/s)	H (m)	H_d (m)	H_d/H	Frd	S
1	30	0.036	0.23	6.4	0.9	0.84
2	30	0.052	0.25	4.81	0.85	0.96
3	30	0.072	0.27	3.75	0.8	0.97
4	30	0.091	0.29	3.19	0.7	0.99
5	40	0.044	0.23	5.2	1.23	0.68
6	40	0.054	0.25	4.6	1.1	0.93
7	40	0.073	0.27	3.7	1	0.96
8	40	0.092	0.29	3.15	0.97	0.98
9	50	0.053	0.23	4.3	1.5	0.57
10	50	0.059	0.25	4.2	1.4	0.85
11	50	0.076	0.27	3.6	1.3	0.92
12	50	0.093	0.29	3.1	1.2	0.97
13	60	0.062	0.23	3.7	1.85	0.48
14	60	0.068	0.25	3.67	1.7	0.74
15	60	0.079	0.27	3.4	1.6	0.89
16	60	0.096	0.29	3.06	1.46	0.94
17	70	0.067	0.23	3.4	2.15	0.45
18	70	0.078	0.25	3.2	2	0.64
19	70	0.088	0.27	3	1.8	0.80
20	70	0.102	0.29	2.84	1.71	0.88
21	30	0.033	0.08	2.42	2.65	–
22	30	0.033	0.13	3.94	1.62	–
23	30	0.033	0.18	5.45	1.17	–
24	40	0.043	0.08	1.86	3.5	–
25	40	0.043	0.13	3.02	2.2	–
26	40	0.043	0.18	4.18	1.57	–
27	50	0.051	0.08	1.56	4.4	–
28	50	0.051	0.13	2.54	2.7	–
29	50	0.051	0.18	3.52	1.96	–
30	60	0.06	0.08	1.33	5.3	–
31	60	0.06	0.13	2.16	3.3	–
32	60	0.06	0.18	3	2.4	–
33	70	0.069	0.08	1.15	6.2	–
34	70	0.069	0.13	1.88	3.8	–
35	70	0.069	0.18	2.6	2.75	–

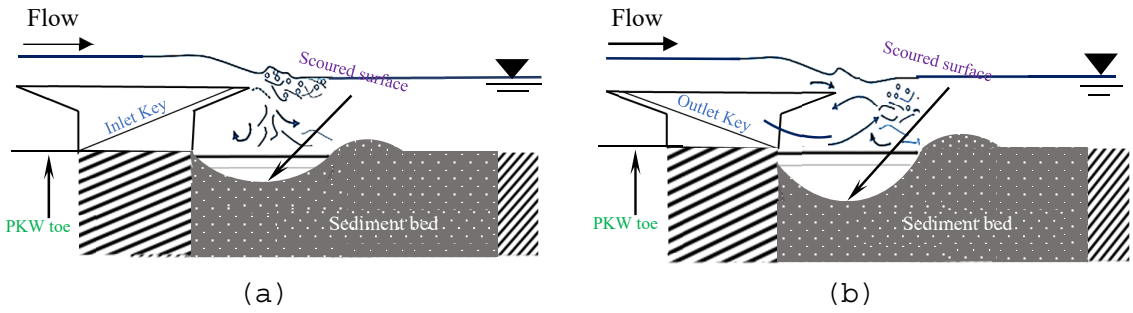


Fig. 2. The submerged flow pattern downstream of: (a) Inlet key, and (b) Outlet key.

Figure 5 presents a typical scour hole development. The scoured sediments were transported downstream to form a sediment ridge (Fig. 5). According to this figure, the scour hole dimensions are smaller in the submerged flow (Test 9) compared to the free flow (Test 27) condition. Over time, the values of maximum scour depth and scour hole length have increased in both the free and submerged flow conditions, while the maximum scour depth occurred at a farther distance from the weir toe because of the increased diffusion length and the consequent jet deflection (Lantz et al., 2022). According to

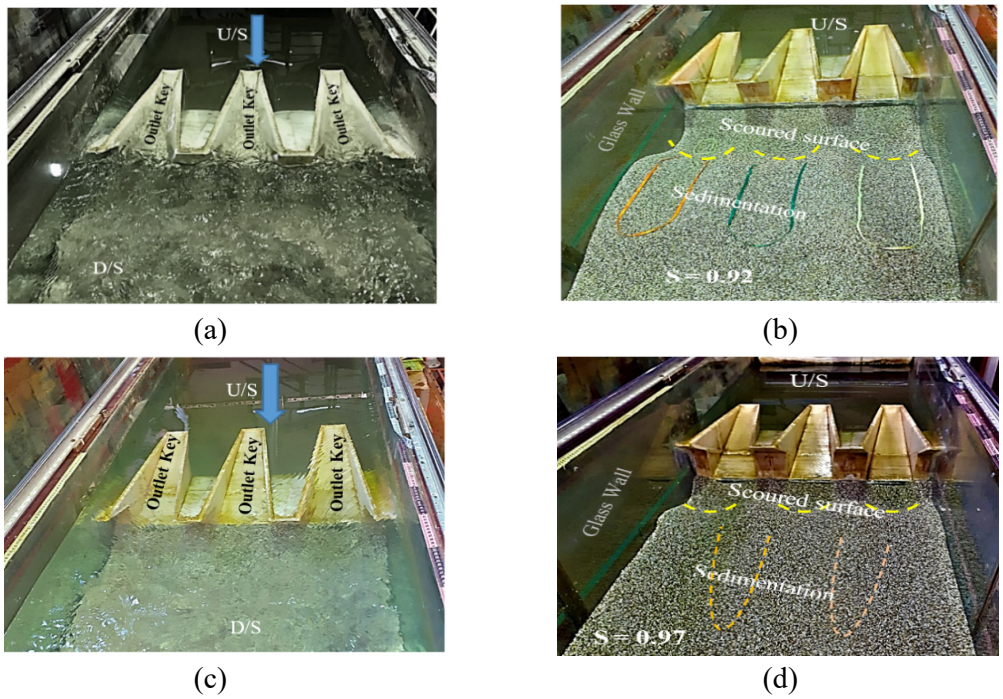


Fig. 3. The flow and bed topography for: a) and b) $S = 0.92$, c) and d) $S = 0.97$; $Q = 50\times10^{-3}$ m^3/s.

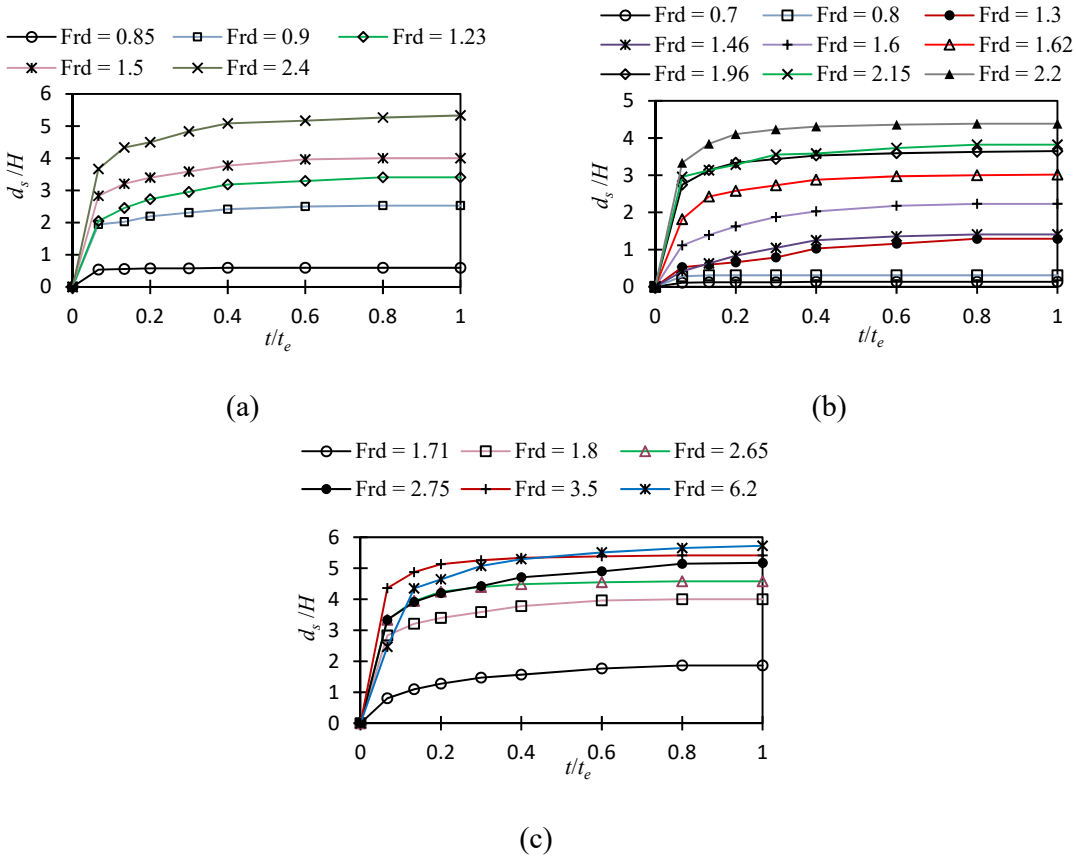
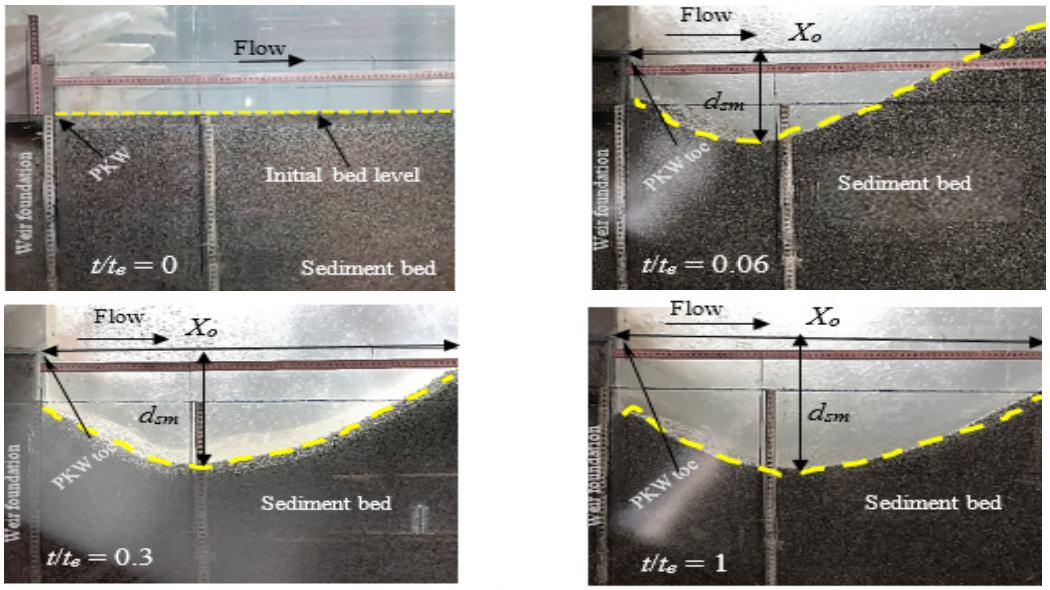
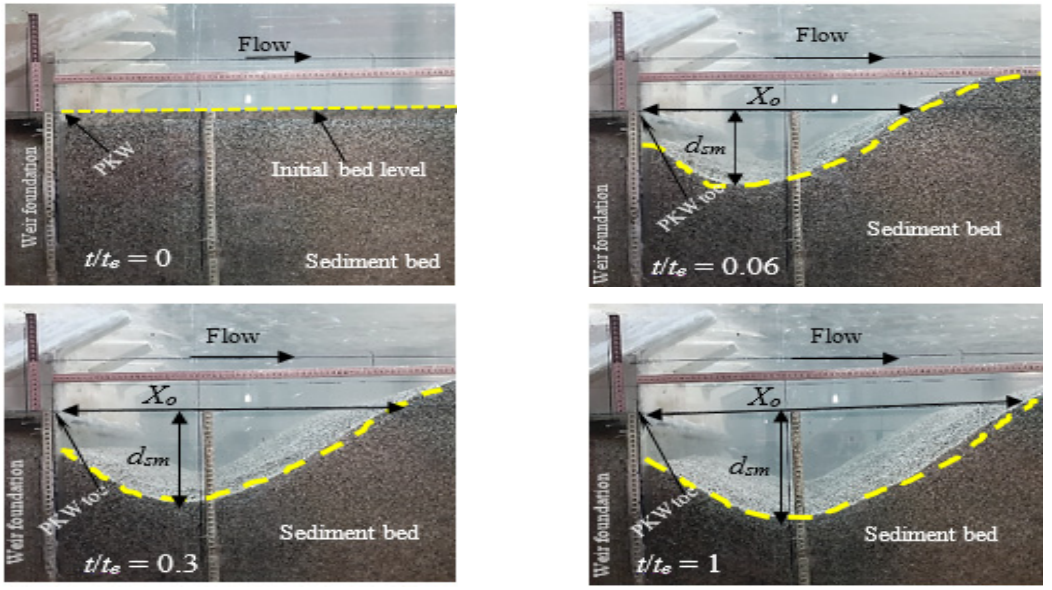


Fig. 4. Temporal evolution of scour depth for: a) $4 < H_d/H < 6.4$, b) $3 < H_d/H < 4$, and c) $1 < H_d/H < 3$.

Fig. 5, after about 2 hours from the start of the test, the scour depth differed by about 19% compared to the maximum scour depth. Most of the changes occurred during the initial 20% time of the experiments. Because the rate of scour decreases with excess shear stress acting on the bed (Lantz et al., 2022). Moreover, the rate of changes was higher in the free flow compared to the submerged flow condition. In the free flow condition, the highest and lowest amounts of the scour depths



(a)



(b)

Fig. 5. Scour development with time for: a) test 9 (Q = 50×10^{-3} m^3/s, H_d = 0.23 m and S = 0.57), b) test 27 (Q = 50×10^{-3} m^3/s and H_d = 0.08 m).

were 0.395 and 0.093 m, which occurred in Test 33 (Q = 70×10^{-3} m^3/s, and H_d = 0.08 m) and Test 23 (Q = 30×10^{-3} m^3/s and H_d = 0.13 m), respectively. While in the submerged flow condition, the highest and lowest scour depths were 0.28 and 0.012 m, which occurred in Test 17 (Q = 70×10^{-3} m^3/s and H_d = 0.23 m) and Test 4 (Q = 30×10^{-3} m3/s and H_d = 0.29 m), respectively.

The effects of discharge and tailwater depth on the location of maximum scour depth are shown in Fig. 6. In this figure, X is the distance from the weir toe in the flow direction, and L is the length of the sedimentary bed along the channel. According to Fig. 6, the maximum scour depth in the submerged and free flow conditions are 0.0005 to 4.43 and 3.8 to 8.15 times the flow head over the weir, respectively. It is also clear that the location of maximum scour depth depends on the discharge and tailwater depth. The maximum scour depth has occurred at a shorter distance from the weir toe in the submerged flow compared to the free flow. This is also due to increased diffusion length downstream of the weir and, consequently, reduced power of the flow to transport the sediments in the submerged flow condition. In both flow conditions, the highest amount of scouring occurred downstream of the outlet keys in most tests.

Figure 7 portrays the bed topography changes for different discharges under the free and submerged flow conditions. Her Y is the lateral distance from the channel wall. In the case of lower discharge and higher submergence ratio (i.e., Q = 30×10^{-3} m^3/s and S = 0.84), as shown in Fig. 7a, it is clear that the sediment ridges were more prominent. The variations of bed topography increased with the discharge enhancement. In the free flow, due

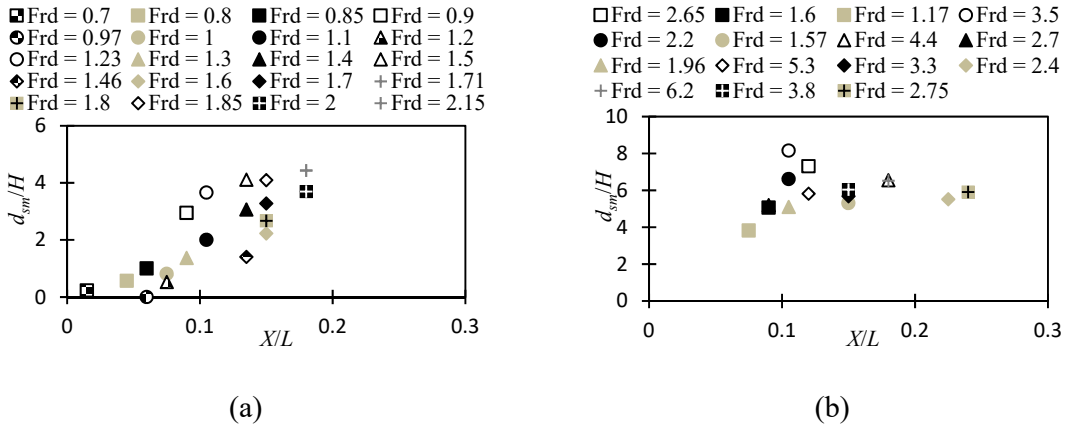


Fig. 6. Location of maximum scour depth for: a) Submerged flow and b) Free flow.

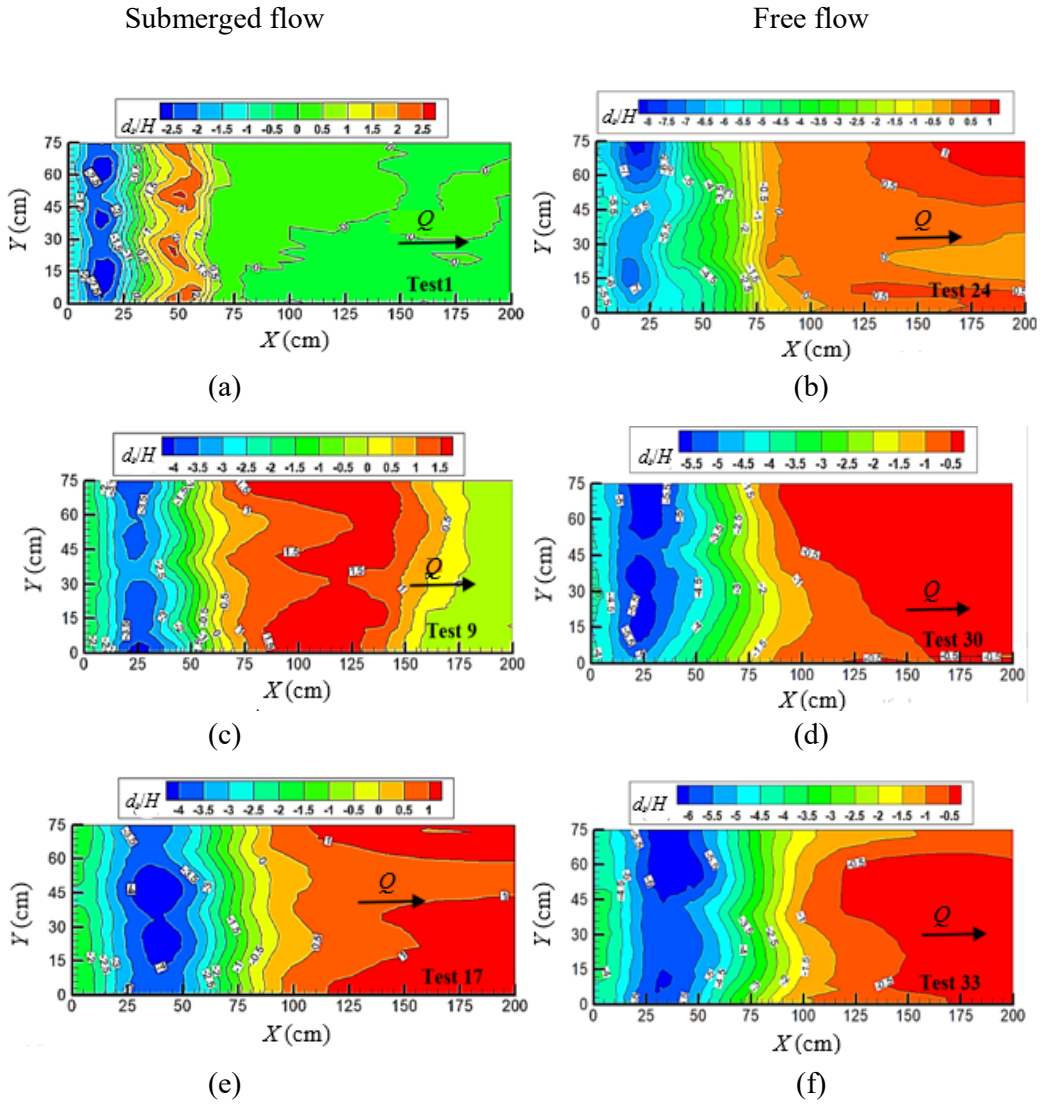


Fig. 7. Equilibrium bed topography for submerged and free flow: a) $Q = 30\times10^{-3}$ m^3/s, $S = 0.84$, b) $Q = 30\times10^{-3}$ m^3/s, c) $Q = 50\times10^{-3}$ m^3/s, $S = 0.57$, d) $Q = 50\times10^{-3}$ m^3/s, e) $Q = 70\times10^{-3}$ m^3/s, $S = 0.45$, and f) $Q = 70\times10^{-3}$ m^3/s.

to higher drop height and greater outflow velocity at the downstream water surface, more changes occurred in the bed topography. The scouring under the submerged flow (Fig. 7a, c and e) and free flow (Fig. 7b, d and f) occurred up to a distance of 0.18 to 0.36 m and 0.21 to 0.30 m from the weir, respectively. Figure 8 shows the typical 3-dimensional topography of the bed

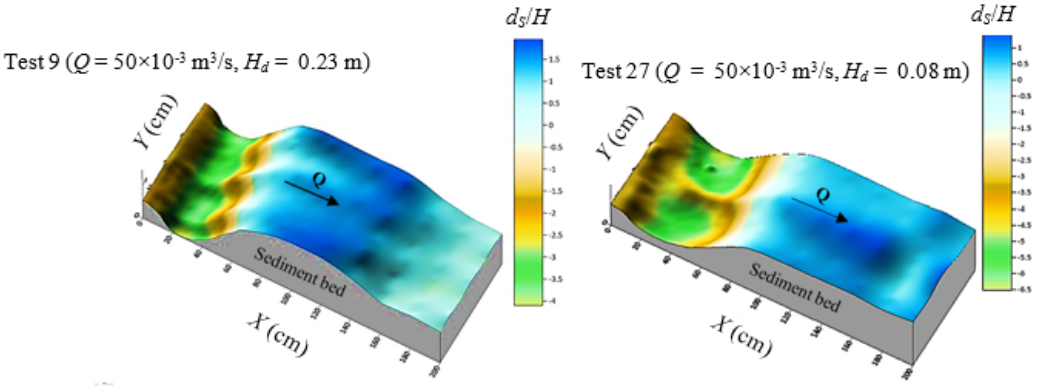
downstream of the weir for the free and submerged flow conditions for discharge of 0.05 m^3/s and tailwater depths of 0.23 and 0.08 m. The differences in the bed topography in the free and submerged flow conditions are also evident in this figure. It is also clear that the volume of the scour hole under the free flow is higher than the submerged flow. The volume of scour hole for Test 9 (Fig. 8a) and Test 27 (Fig. 8b) is 0.053 and 0.12 m^3, respectively. It is also clear that the sediment ridge under the submerged flow condition occurred closer to the weir toe, which reduced the sediment transport capacity of the flow. Table 2 shows the changes in the volume and area of scour hole in the free flow and submerged flow conditions. The average changes in the volume and area of the scour hole in the free flow are 0.103 m^3 and 0.12 m^2, and in the submerged flow are 0.025 m^3 and 0.042 m^2, respectively. The scour hole volume and scour hole area in the submerged flow are 0.248 and 0.35 times their corresponding values in the free flow.

Figure 9 shows the longitudinal bed profiles for different discharges and submergence ratios. It is evident from this figure that the trend of bed variations under different hydraulic conditions is somewhat the same along the channel. However, the bed profile variations are higher, with the lowest submergence ratio. It is also clear that the scour begins from the weir toe. By increasing the submergence ratio, the maximum scour depth occurred closer to the weir toe, while the scour depth and scour hole length values decreased. Enlargement of the scour hole by increasing the discharge is also evident in Fig. 9. Almost no scouring occurred for discharge of 0.03 m^3/s with the submergence ratio of 0.99 (i.e., for Test 1). With the increase in the discharge, due to the increased scouring potential of the flow, scouring occurs with a greater depth and farther from the weir toe. With increases of 18, 44, 70, 96 and 95% in the submergence ratio for the discharges of 0.03, 0.04, 0.05, 0.06 and 0.07 m^3/s, the relative scour depth (d_s/H) was reduced by 92, 86, 89, 65 and 56%, respectively.

Figure 10 shows the effect of particle Froude number on the longitudinal bed profiles for different tailwater depths. It is clear from this figure that the maximum scour depth, its distance from the weir toe, and the scour hole length have increased with the increase in the particle Froude number. By increasing the particle Froude number, due to increased outflow velocity, the scoring potential of the flow has increased and caused the increased dimensions of the scour hole. At higher particle Froude numbers, the location of maximum scour has occurred at a farther distance from the weir toe. With increases of 130, 138, 129, 144, 135, 125, and 144% in the particle Froude number for

Table 2. Comparison of scour volume (V) and area (A).

Test No.	$V\times10^{-2}$ (m^3)	Average	$A\times10^{-1}$ (m^2)	Average
1	0.975		2.437	
2	0.487		1.282	
3	0.231		0.744	
4	0.103		0.295	
5	2.454		3.958	
6	1.443		2.328	
7	0.822		1.326	
8	0.453		0.731	
9	4.750		5.600	
10	2.889	2.549	2.772	4.229
11	1.608		1.878	
12	0.819		1.412	
13	7.169		12.360	
14	3.628		5.272	
15	1.95		4.178	
16	1.27		3.012	
17	10.82		18.650	
18	4.56		7.992	
19	2.49		4.523	
20	2.06		3.830	
21	5.95		13.395	
22	3.5		8.994	
23	1.95		7.078	
24	9.94		20.299	
25	6.44		13.355	
26	4.04		9.997	
27	12.42		18.921	
28	9.85	10.258	12.364	12.049
29	7.15		12.370	
30	16.85		23.983	
31	15.45		22.388	
32	11.62		17.591	
33	18.53		30.88	
34	16.07		27.71	
35	14.11		23.92	



(a) (b)

Fig. 8. Three-dimensional bed topography downstream of weir for: a) Submerged flow and b) Free flow.

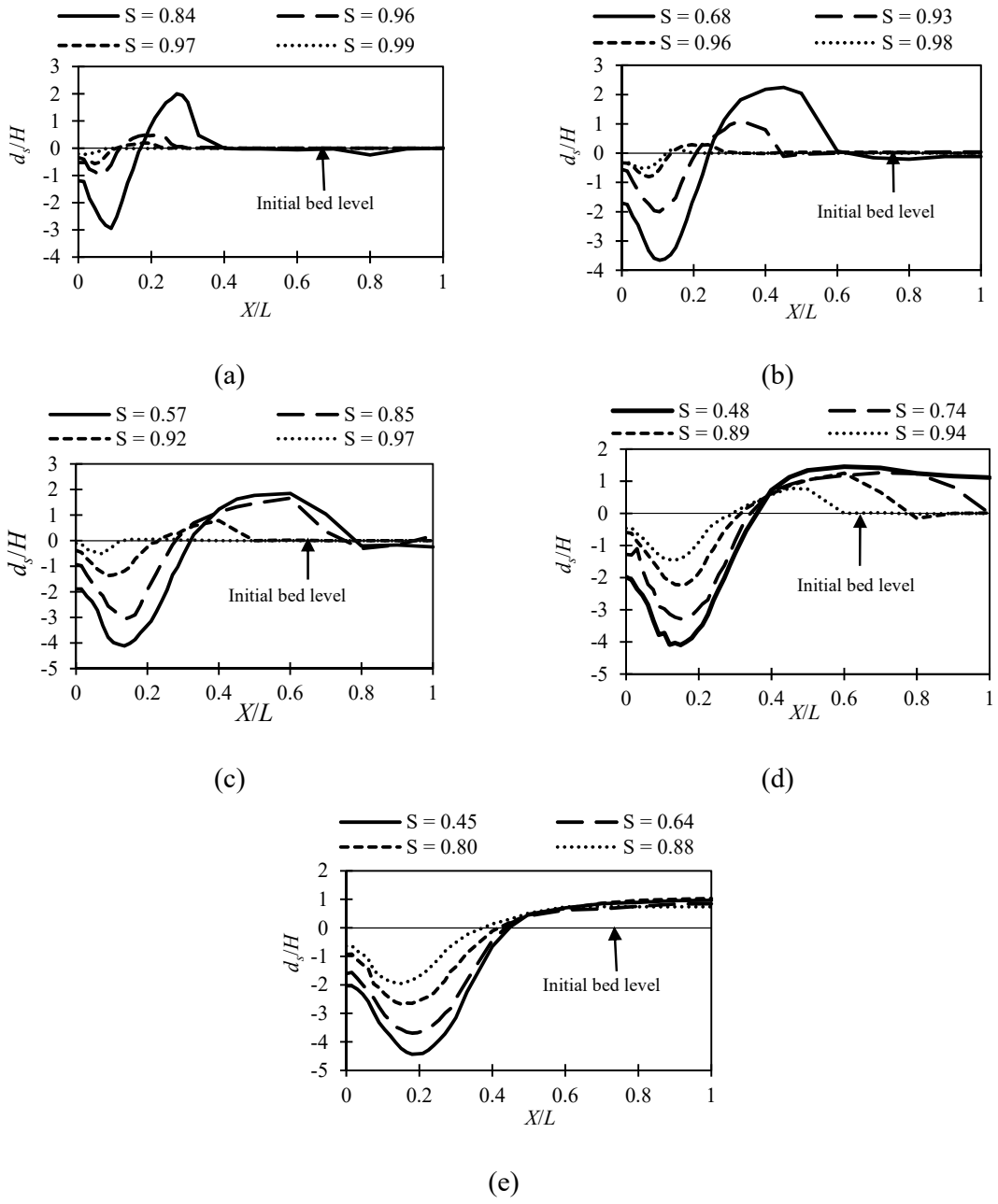


Fig. 9. Effect of submergence ratio on the longitudinal bed profile for discharge of: a) 30×10^{-3} m^3/s, b) 40×10^{-3} m^3/s, c) 50×10^{-3} m^3/s, d) 60×10^{-3} m^3/s, and e) 70×10^{-3} m^3/s.

Table 3. Specifications of the PKWs and the flow used by Yazdi et al. (2020) and Ghafouri et al. (2020).

Parameters	P (m)	L (m)	W (m)	W_i (m)	W_o (m)	B (m)	B_b (m)	$B_i = B_o$ (m)	T_s (m)	N	Q (m^3/s)	h_d (m)	Frd
Yazdi et al. (2020)	0.15	2.39	0.50	0.0455	0.0342	0.35	0.15	0.10	0.004	3	0.0195–0.0325	0–0.05	0.8–1.95
Ghafouri et al. (2020)	0.20	3.30	0.75	0.175	0.051	0.50	0.25	0.125	0.012	3	0.03–0.50	0.13-0.18	1.5–3.5

the tailwater depths of 0.08, 0.13, 0.18, 0.23, 0.25, 0.27, and 0.29 m, the distances of maximum scour depth from the weir toe have increased by 50, 67, 220, 100, 200, 233, and 900%, respectively.

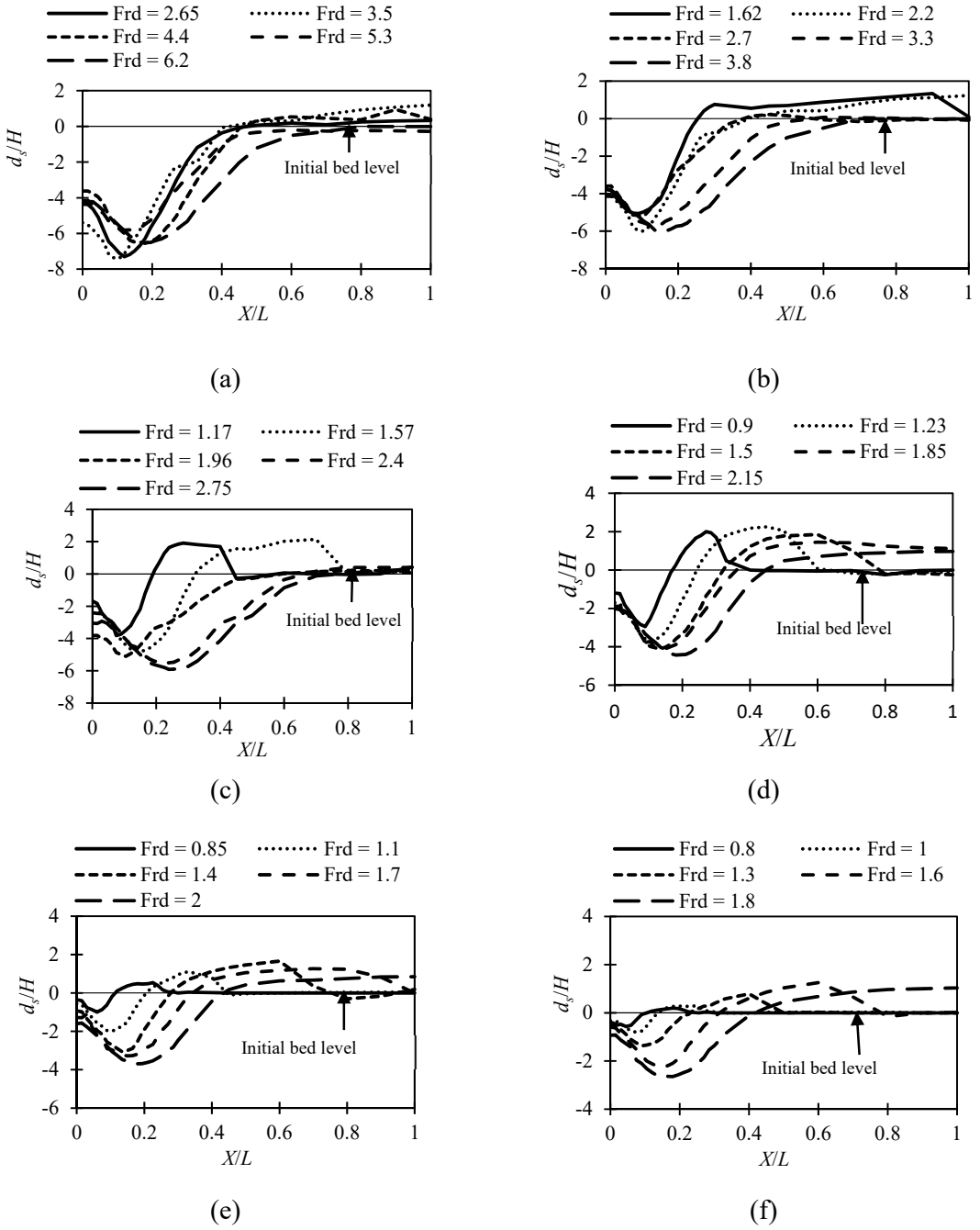


Fig. 10. Effect of particle Froude on longitudinal bed profile at tailwater depth: (a) 0.08, (b) 0.13, (c) 0.18, (d) 0.23, (e) 0.25 and (f) 0.27 m.

On the other hand, for lower tailwater depths (Fig. 10a and b), due to higher drop height and the increased scouring potential of flow, the dimensions of the scour hole are larger compared to higher tailwater depths (Fig. 10d and e). Figure 10 also shows that increasing the particle Froude number, due to increased flow velocity and the sediment carrying capacity, the dimensions of sediment ridge reduced, especially at higher tailwater depths (Fig. 10e and f). In addition, the sediment ridge with a flatter surface and longer length occurred at the higher particle Froude numbers. In general, the ridge height increased by increasing the particle Froude numbers. The lower sedimentation height occurred at the higher tailwater depths and lower particle Froude numbers (Figs. 10e and f). The sedimentation in the free flow is less than the submerged flow, such that in all the discharges, the maximum level of sedimentation in the free flow was 50.6% less than the submerged flow.

Based on Eqs. (3) and (4), the effects of particle Froude number on the geometric parameters of the scour hole are shown in Fig. 11 for the free and submerged flow conditions. The data obtained by Yazdi et al. (2020) and Ghafouri et al. (2020) were also added for comparison in this figure. Table 3 presents the characteristics of the trapezoidal PKW and the flow used by these researchers. The higher values of the relative scour parameters for the free flow condition are evident from Fig. 11. Generally, the average values of maximum relative scour depths under the free flow are about 58.5% higher than the submerged

flow. In both the free and submerged flow conditions, the relative scour parameters increased with the increase of the particle Froude number (Fig. 11a–d). Furthermore, at a constant particle Froude number, the relative scour hole lengths were greater under the free flow than the submerged flow. This enhancement was more evident in the particle Froude numbers greater than 3. The location of maximum scour depth from the weir toe and the scour hole length under the free flow, on average, were 62 and 189.5% more than those under the submerged flow (according to Fig. 11c). In addition, according to Fig. 11b, the relative scour depth at the weir toe was higher by 307% in the free flow compared to the submerged flow.

3.1 Equations for scour parameters

It is important to predict the geometric dimensions of the scour hole to ensure weir stability and implement measures for its downstream bed protection. Based on the analysis of data, Eq. (5) was selected for estimating the geometric characteristics of the scour hole downstream of the trapezoidal PKW for the free flow:

$$\frac{\psi}{H}=K\ (\mathrm{Frd})^{a}\left(\frac{H_d}{H}\right)^{b} \tag{5}$$

K, a, and b are the empirical constants for the free flow condition. Using non-linear regression and laboratory data, these constant values were obtained using the present data and those obtained by Yazdi et al. (2020) and Ghafouri et al. (2020), as presented in Table 4. The accuracy of Eq. (5) was evaluated by using the statistical indices of correlation coefficient R^2, the mean absolute error MAE, and the average percentage error E (Eqs. (6) to (8)). The values of these statistical indices due to Eq. (5) are calculated and presented in Table 4.

$$\mathrm{R}^2=\frac{\sum_{i=1}^{N}(M_i*C_i)}{\sqrt{\sum_{i=1}^{N}(M_i)^2\sum_{i=1}^{N}(C_i)^2}} \tag{6}$$

$$\mathrm{MAE}=\frac{\sum_{i=1}^{N}\left|(C_i-M_i)\right|}{\mathrm{N}} \tag{7}$$

$$\mathrm{E}=\frac{100}{\mathrm{N}}\sum_{i=1}^{N}\left|\frac{C_i-M_i}{M_i}\right| \tag{8}$$

here M_i and C_i represent the observed and calculated values of the scour parameters, respectively, and N is the number of data.

Figure 12 shows the accuracy of Eq. (5) for estimating the scour parameters for the present data and the data of Yazdi et al. (2020) and Ghafouri et al. (2020). This Figure and Table 4 show the good accuracy of Eq. (5) for the free flow condition.

Table 4. Statistics indices due to Eq. (5) for Free flow.

Ψ	K	a	b	R^2	MAE	E
d_{sm}	1.02	1.01	0.71	0.997	0.112	3.47
Z_f	1.84	0.64	0.015	0.997	0.004	0.10
L_{xm}	0.52	1.29	1.18	0.993	0.038	1.57
X_o	0.08	3.05	2.72	0.998	0.148	1.43

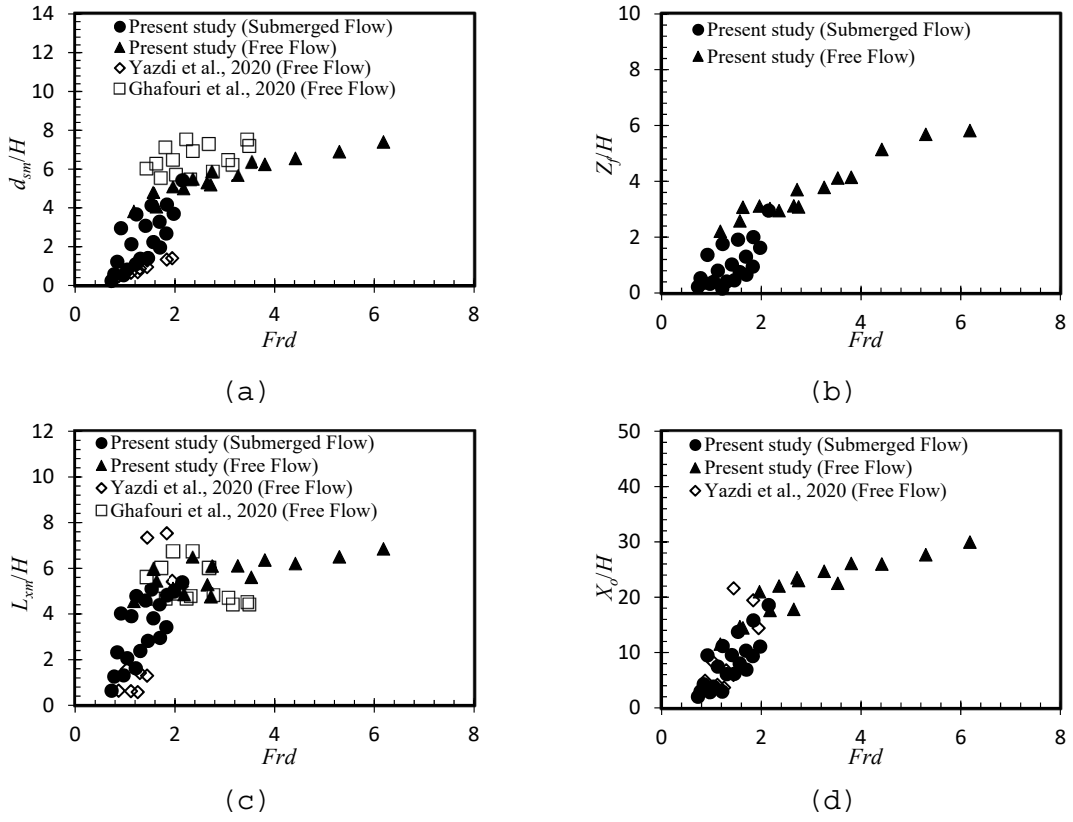


Fig. 11. Comparison of scour parameters: a) Maximum scour depth, b) Weir toe scour depth, c) Maximum scour depth location, and d) Scour hole length.

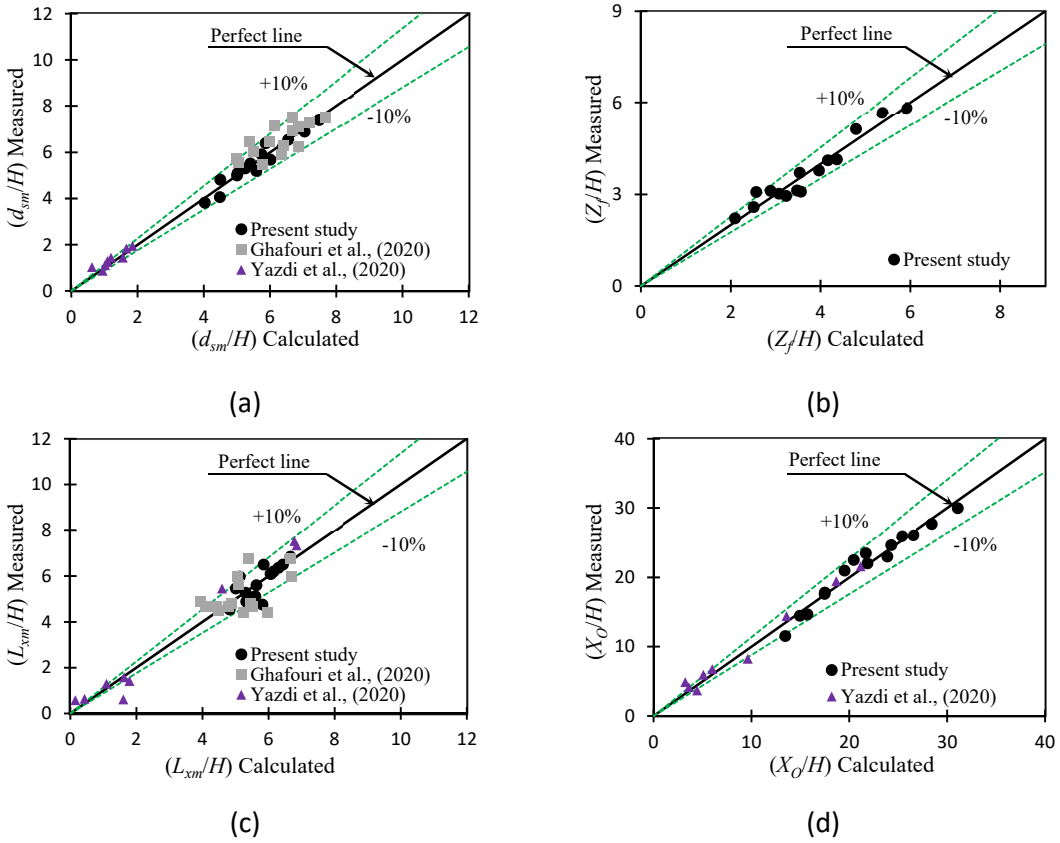


Fig. 12. Comparison between measured and computed scour parameters for free flow: a) Maximum scour depth, b) Weir toe scour depth, c) Maximum scour depth location and d) Scour hole length.

For the submerged flow condition, Eq. (5) is written as:

$$\frac{\psi}{H}=K_1K\left(\mathrm{Frd}\right)^a\left(\frac{H_d}{H}\right)^b\left(S\right)^c \quad (9)$$

Here, K_1 and c are the empirical constants obtained using the experimental data for the submerged flow condition (Table 5). The values of statistical indices of R^2, MAE, and E due to Eq. (9) are calculated and presented in Table 5. Equations (5) and (9) are valid for $0.7 \le \mathrm{Frd} \le 6.2$, $1 < H_d/H < 6.4$, and $0.48 \le S < 1$.

Figure 13 compares the calculated values of the scour parameters using the obtained equation and their corresponding observed values for the submerged flow condition. This figure and the values of statistical indices given in Table 5 also represent the good accuracy of Eq. (9) for the submerged flow condition.

4 CONCLUSION

One of the important issues in the stability of weirs is their downstream scouring. In this experimental research, the geometry of the scour hole downstream of a trapezoidal PKW was investigated with varying discharges and tailwater depths under free and submerged flow conditions. The results revealed that the scour characteristics depend on the discharge, tailwater depth, and submergence ratio. The main results are as follows:

– With increasing the particle Froude number, the geometric features of the scour hole were enhanced.

– The values of scour hole parameters were more under free flow than submerged flow.

– With increasing submergence ratio, scour depth and scour hole length showed a decreasing trend. Almost no scouring occurred at particle Froude number of 0.9 and submergence ratio of 0.99.

– On average, maximum scour depth, distance of the location of maximum scour depth from the weir toe, scour hole length, and weir toe scour depth under the free flow increased by 58.5, 62, 189.5, and 307%, compared to those of the submerged flow, respectively.

– The maximum scour depth varied between 0.005 to 4.43 and 3.8 to 8.15 times the approach flow depth under submerged and free flow conditions, respectively.

– With an increase of 130, 138, 129, 144, 135, 125, and 144% in particle Froude number at tailwater depths of 0.08, 0.13, 0.18, 0.23, 0.25, 0.27, and 29 0.0 m, distances of maximum scour depth from the weir toe were increased by 50, 67, 220, 100, 200, 233, and 900%, respectively.

– The greatest weir toe scour depth decrease occurred at the lowest submergence ratio.

– Most scouring occurred in the first 20% of the test duration. The changes were higher in the free compared to the submerged flow. After about 2 hours, the scour depth differed by 19% from the maximum scour depth.

– The scour hole volume and scour hole area in the submerged flow are 0.248 and 0.35 times their corresponding values in the free flow.

– New equations obtained to estimate the scour parameters showed good statistical indices of R^2, MAE, and E based on the present data and those obtained by previous researchers.

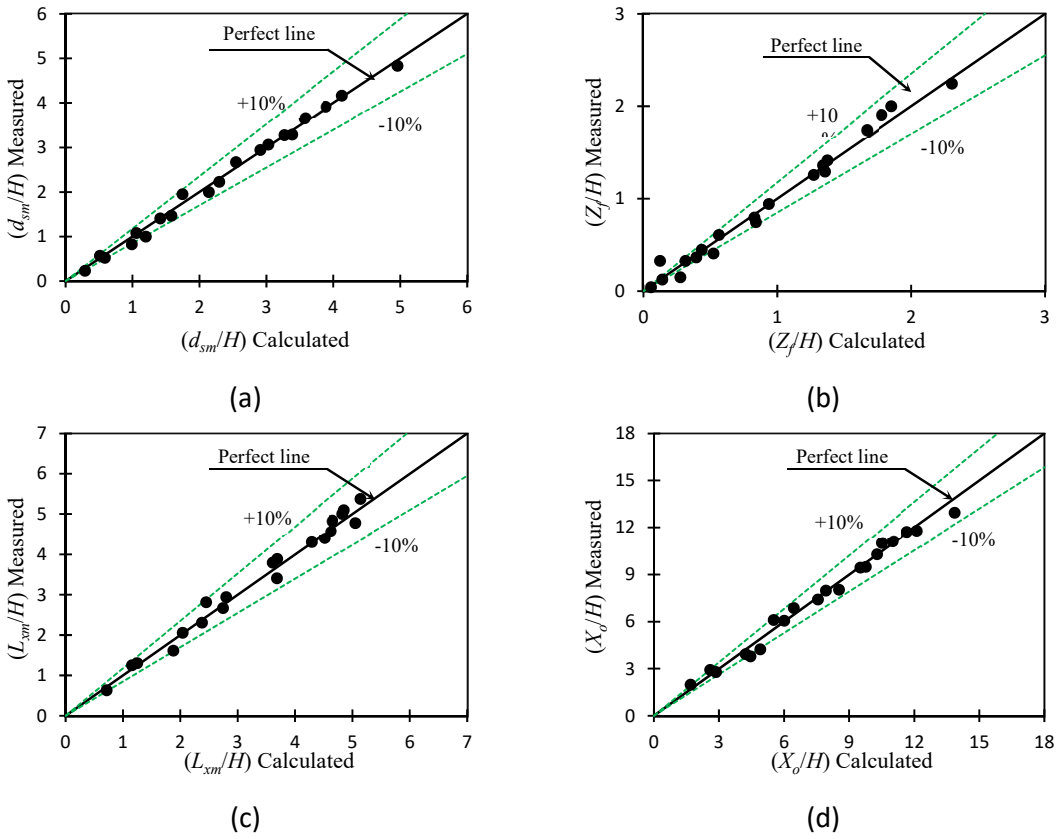


Fig. 13. Comparison between measured and computed scour parameters for submerged flow: a) Maximum scour depth, b) Weir toe scour depth, c) Maximum scour depth location and, d) Scour hole length.

Table 5. Statistics indices due to Eq. (9) for Submerged flow.

ψ	K_1	c	R^2	MAE	E
d_{sm}	0.04	0.02	0.999	0.019	3.25
Z_f	0.01	0.05	0.997	0.006	4.34
L_{xm}	0.21	0.39	0.998	0.033	0.15
X_o	2.05	0.04	0.998	0.078	0.86

NOMENCLATURE

The following symbols are used in this paper:
A = area of scour hole (m^2);
a = empirical constant (–);
B = side wall crest length (m);
b = empirical constant (–);
B_i = overhang length for the inlet key (m);
B_o = overhang length for the outlet key (m);
C_i = calculated values;
c = empirical constant;
d_{10} = sediment size corresponding 10% finer;
d_{50} = mean sediment size (m);
d_{90} = sediment size corresponding to 90% finer (m);
d_s = scour depth (m);
d_{sm} = maximum scour depth (m);
E = average percentage error;
Frd = particle Froude number (–);
g = acceleration due to gravity (m/s^2);
H = upstream total head (m);
H^*_d = tailwater total head for submerged flow with respect to weir crest (m);
H_d = tailwater total head (m);
h = upstream head (m);
h_d = tailwater depth (m);
h_{sm} = maximum height of sedimentary ridge (m);
K = empirical constant;
K_1 = empirical constant;
L = length of sedimentary bed along the channel (m);
L_w = length of weir crest (m);
L_x = scour depth location along the x-axis (m);
L_{xm} = maximum scour depth location along the x-axis (m);
MAE = mean absolute error;
M_i = observed value;
N = number of PKW cycles;
P = weir height (m);
Q = weir discharge (m^3 /s or L/s);
q = unit discharge (m^2 /s);
R^2 = correlation coefficient;
S = submergence ratio (–);
t = time (min);
t_e = time to equilibrium (min);
T_s = weir wall thickness (m);
V = flow velocity (m/s);
V = volume of scour hole (m^3);
W = channel width (m);
W_i = PKW inlet key width (m);
W_o = PKW outlet key width (m);
X = distance from weir toe in the direction of flow (m);
X_o = scour hole length (m);
Y = transverse distance from the channel wall (m);
Z_f = depth of scour at the weir toe (m);

ρ = specific mass of fluid (kg/m^3);
ρ_s = specific mass of sediment particles (kg/m^3);
σ = surface tension of water (N/m);
σ_g = standard deviation (–);
μ = dynamic viscosity of water (Ns/m^2);
ψ = geometric characteristics of scour hole and
ΔH = change in upstream to downstream head (m).

REFERENCES

Abdi-Chooplou, C., Bodaghi, E., Ghodsian, M., Vaghefi, M., 2022a. Temporal evolution of scouring downstream of a trapezoidal PKW. International Journal of River Basin Management, 20, 1–14. DOI: 10.1080/15715124.2022.2143513

Abdi-Chooplou, C., Ghafouri, A., Ghodsian, M., Vaghefi, M., 2022b. Local scour downstream of type-A trapezoidal piano key weir. In: Proc. 9th IAHR International Symposium on Hydraulic Structures. Utah State University, Logan, Utah, USA, 10 p. https://digitalcommons.usu.edu/ishs/2022/all2022/21

Abdi-Chooplou, C., Ghodsian, M., Abediakbar, D., Ghafouri, A., 2023. An experimental and numerical study on the flow field and scour downstream of rectangular piano key weirs with crest indentations. Innovative Infrastructure Solutions, 8, 5, 140. https://doi.org/10.1007/s41062-023-01108-7

Abhash, A., Pandey, K.K., 2021. Numerical study of discharge-head relationship of piano key weirs for low heads. Water Resources, 48, 2, 235–244. https://doi.org/10.1134/S0097807821020020

Barcouda, M., Cazaillet, O., Cochet, P., Jones, B.A., Lacroix, S., Laugier, F., Odeyer, C., Vingny, J.P., 2006. Cost-effective increase in storage and safety of most dams using fuse gates or PK weirs. In: Proc. 22nd ICOLD Congress. Barcelona, Spain.

Bodaghi, E., Ghodsian, M., Abdi-Chooplou, C., 2021. Experimental study on the effect of discharge and tailwater depth on scour downstream of a piano key weir. In: Proc. 20th Iranian Hydraulic Conf. Gorgan University of Agriculture Sciences and Natural Resources, Iran. (In Persian.)

Bodaghi, E., Ghodsian, M., Abdi-Chooplou, C., 2023. The experimental study of downstream scouring of trapezoidal piano key weir type A under free and submerged flows. Journal of Hydraulics, Iranian Hydraulic Association, 18, 1, 1–18. https://doi.org/10.30482/jhyd.2022.330389.1590. (In Persian.)

Chiew, Y.M., 1984. Local scour at bridge piers. Rep. No. 355. Department of Civil Engineering, University of Auckland, Auckland, New Zealand.

Chiew, Y.M., Melville, B., 1989. Local scour at bridge piers with non-uniform sediments. Proceedings of the Institution of Civil Engineers, Part 2, 87, 2, 215–224. https://doi.org/10.1680/iicep.1989.2004

Dabling, M.R., Tullis, B.P., 2012. Piano key weir submergence in channel applications. J. Hydrol., 138, 7, 661–666. https://doi.org/10.1061/(ASCE)HY.1943-7900.0000563

Dehrashid, F.A., Gohari, S., 2019. Experimental study of downstream scour of piano keys weirs. Journal of Water and Soil Conservation, 26, 1, 91–109. https://www.sid.ir/en/journal/ViewPaper.aspx?id=728702 (In Persian.)

Erpicum, S., Nagel, V., Laugier, F., 2011. Piano key weir design of Ravage dam. In: Proc. Int. Conf. Labyrinth and piano key weirs. CRC Press, London, pp. 43–50.

Ettema, R., Arndt, R., Roberts, P., Wahl, T., 2000. Hydraulic modelling: concepts and practice, ASCE manuals and reports on engineering practice no. 97. American Society of Civil Engineers, Reston, VA, USA, 10, 9780784404157.

Ghafouri, A., Ghodsian, M., Abdi-Chooplou, C., 2020. Experimental study on the effect of discharge and tailwater depth on bed topography downstream of a piano key weir, Journal of Hydraulics, 15, 3, 107–122. DOI: 10.30482/jhyd.2020.236770.1465 (In Persian.)

Ghodsian, M., Abdi-Chooplou, C., Ghafouri, A., 2021. Scouring downstream of triangular and trapezoidal pianos key weir. Journal of Hydraulics, Iranian Hydraulic Association, 16, 2, 43–58. https://doi.org/10.30482/jhyd.2021.261439.1497. (In Persian.)

Hien, T.C., Son, H.T., Khanh, M.H.T., 2006. Results of some piano keys weir hydraulic model tests in Vietnam. In: Proc. 22nd ICOLD Congress. CIGB/ICOLD, Barcelona, Q87(R39), pp. 581–596.

Jüstrich, S., Pfister, M., Schleiss, A.J., 2016. Mobile riverbed scours downstream of a piano key weir. J. Hydrol., ASCE, 142, 11, 04016043. https://doi.org/10.1061/(ASCE)HY.1943-7900.0001189

Kabiri-Samani, A., Javaheri, A., 2012. Discharge coefficients for free and submerged flow over piano key weirs. J. Hydrol., 50, 1, 114–120. https://doi.org/10.1080/00221686.2011.647888

Karimi, M., Attari, J., Saneie, M., Ghazizadeh, M.R.J., 2019. Side weir flow characteristics: Comparison of piano key, labyrinth, and linear types. J. Hydrol., 144, 12, 04018075. https://doi.org/10.1061/(ASCE)HY.1943-7900.0001539

Kumar, B., Ahmad, Z., 2020. Experimental study on scour downstream of a piano key weir with nose. In: Proc. 8th IAHR International Symposium on Hydraulic Structures. The University of Queensland, Brisbane, Queensland, Australia. https://doi.org/10.14264/uql.2020.595

Kumar, B., Kadia, S., Ahmad, Z., 2021. Sediment movement over type A piano key weir. J. Irrig. Drain. Eng., 147, 6, 04021018. https://doi.org/10.1061/(ASCE)IR.1943-4774.0001561

Lantz, W., Crookston, B.M., Palermo, M., 2021. Apron and cutoff wall scour protection for piano key weirs. Water, 13, 17, 2332. https://doi.org/10.3390/w13172332

Lantz, W.D., Crookston, B.M., Palermo, M., 2022. Evolution of local scour downstream of type A PK weir in non-cohesive sediments. J. Hydrol. Hydromech., 70, 1, 103–113. https://doi.org/10.2478/johh-2021-0035

Laugier, F., 2007. Design and construction of the first piano key weir (PKW) spillway at the Goulours dam. International Journal of Hydropower and Dams, 14, 5, 94–101.

Lempérière, F., Ouamane, A., 2003. The piano keys weir: a new cost-effective solution for spillways. International Journal of Hydropower and Dams, 10, 5, 144–149.

Lempérière, F., Vigny, J.P., Ouamane, A., 2011. General comments on labyrinth and piano key weirs: The past and present. In: Proc. Int. Conf. Labyrinth and piano key weirs. Liege, Belgium, pp. 17–24.

Machiels, O., 2012. Experimental study of the hydraulic behavior of piano key weirs. PhD Thesis. Faculty of Applied Science, University of Liege.

Machiels, O., Erpicum, S., Archambeau, P., Dewals, B.J., Pirotton. M., 2012. Piano key weir preliminary design method - Application to a new dam project. In: Proc. Int. Conf. Labyrinth and piano key weirs, Liege, Belgium, pp. 199–206.

Machiels, O., Erpicum, S., Dewals, B., Archambeau, P., Pirotton, M., 2011. Experimental observation of flow characteristics over a piano key weir. Journal of Hydraulic Research, IAHR, 49, 3, 359–366.

Moradi, S., Shahsavari, H., Esmaili, K., 2020. Investigate foundation local scour type-A piano key weirs with zigzag sidewall. Journal of Hydraulics, Iranian Hydraulic Association, 15, 4, 81–94. https:// doi.org/10.30482/jhyd.2020.251894.1480 (In Persian.)

Ouamane, A., Lempérière, F., 2006. Design of a new economic shape of weir. In: Proc. International Symp. on Dams in the Societies of the 21th Century, 18, pp. 463–470.

Pagliara, S., Hager, W.H., Minor, H.E., 2006. Hydraulics of plane plunge pool scour. Journal of Hydraulic Engineering, 132, 5, 450–461. https://doi.org/10.1061/(ASCE)0733-9429(2006)132:5(450)

Pfister, M., Battisacco, E., De Cesare, G., Schleiss, A.J., 2013. Scale effects related to the rating curve of cylindrically crested piano key weirs. In: Proc. Int. Conf. Labyrinth and piano key weirs II. CRC/Balkema, Leiden, Netherlands, pp. 73–82.

Safarzadeh, A., Noroozi, B., 2015. 3D hydrodynamics of trapezoidal piano key spillways. International Journal of Civil Engineering, 15, 1, 89–101. https:// doi.org/10.1007/s40999-016-0100-8

Yazdi, A.R., Hoseini, S.A., Nazari, S., Amanian, N., 2020. Comparison of downstream scour of the rectangular and trapezoidal piano key weirs. Journal of Hydraulics, Iranian Hydraulic Association, 15, 2, 95–102. https://doi.org/10.30482/jhyd.2020.227522.1453. (In Persian.)

Received 27 April 2023
Accepted 18 October 2023